(Received 29 January 2024, Accepted 1 March 2024, Scheduled 26 March 2024)

A 4-Port Broadband High-Isolated MIMO Antenna for Wireless Communication

Ayyaz Ali[1,*], Maryam Rasool[1], Muhammad Zeeshan Zahid[1], Imran Rashid[1], Adil Masood Siddique[1], Moazzam Maqsood[2], and Farooq Ahmad Bhatti[1]

[1] *Department of Electrical Engineering, Military College of Signals National University of Sciences and Technology, Islamabad, Pakistan*
[2] *Department of Electrical and Computer Engineering Pak–Austria Fachhochschule: Institute of Applied Sciences and Technology, Haripur-KPK, Pakistan*

ABSTRACT: This article proposes a versatile Multiple Input Multiple Output (MIMO) antenna designed for contemporary wireless systems spanning frequencies from 3 to 20 GHz. It serves applications such as 5G mobile, WiFi, WiFi-6E, X-band, partial Ku, and K-band. The original single-element antenna evolves into a 4×4 MIMO configuration with optimized ground plane modifications for enhanced performance. A decoupling structure achieves over 20 dB isolation between inter-elements. The feeding structure, featuring a gradually changing design connected to the antenna's radiating structure, achieves wide bandwidth characteristics. This is further improved by a partial ground structure and slots on the radiating element. The lower frequency band of 3 to 7 GHz is attained with a rectangle-shaped radiator, while semi-circular microstrip lines atop the radiator enable the higher frequency bands of 8 to 15.4 and 18.7 to 20 GHz. The slots and ground structure enhance impedance bandwidth, and semicircles improve the radiation pattern. The MIMO antenna demonstrates measured peak gains of 6.23 dBi at 11.5 GHz, maintaining a radiation efficiency exceeding 80%. Validation through metrics like ECC, DG, CCL, and TARC confirms strong agreement between simulated and experimental results, positioning the MIMO antenna as a robust choice for various wireless communication applications.

1. INTRODUCTION

The telecommunications sector is under demands to enhance its performance and provide more effective tools for connecting a rapidly growing and evolving world. Recognizing this crucial demand, scientists are actively addressing existing technological challenges by devising innovative solutions and making state-of-the-art technology accessible to a wider audience. This imperative has also motivated researchers to explore beyond existing constraints and develop technology that better serves consumers. Advancements in wireless systems necessitate improved high-speed and reliable data transmission capacity [1]. The scientific community has proposed various methods to meet this demand, one of which is Multiple Input Multiple Output (MIMO) system [2]. MIMO systems offer increased channel capacity, enhanced link reliability, and high data rates in wireless communication through the use of multiple radiating elements, rendering them less susceptible to multipath fading. However, optimal performance and low correlation values necessitate proper configuration and high isolation between the multiple antenna elements while maintaining a small antenna size [3, 4]. The literature explores several techniques to enhance isolation between antenna elements, including defective ground structures (DGSs), decoupling networks, neutralization lines, pattern diversity, and polarization diversity [5, 6]. Numerous antenna designs have been presented in the literature. For instance, in study [7], an Ultra-Wideband (UWB) MIMO antenna system features a jug-shaped radiating element incorporating a semicircle-shaped strip and a C-shaped stripline, achieving exceptional impedance matching and an ultra-wide bandwidth. Additionally, [8] details a 4-port UWB MIMO antenna design utilizing a circular radiator with six circular slits arranged at a 60-degree angle, maintaining ultra-wide bandwidth and impedance matching. Similar UWB MIMO antennas in [9–11] utilize circular and vertical striplines on the radiating element, along with defective ground structures, to achieve ultra-wide bandwidth while ensuring a compact antenna size. The literature also introduces dual-band MIMO antennas, such as the ones discussed in [12] and [13], featuring slotted quarter-circle-shaped antenna elements and a thin microstrip line, respectively. Moreover, a MIMO tri-band asymmetric coplanar strip (ACS)-fed coplanar antenna is presented in [14], showcasing a monopole antenna with L-shaped extensions and a curving microstrip line for operating across multiple bands. In [15], a wideband four-port MIMO antenna employs circular slits on the top side and a grounding arrangement on the bottom surface, achieving the desired wideband characteristic. Similarly, [16] describes a wideband MIMO antenna with enhanced radiation performance and impedance bandwidth through an EL-shaped slit and two stubs in the ground structure. Another compact wideband MIMO antenna is discussed in [17], featuring dual-polarized structures and a T-shaped stripline with a rotated square-shaped slot in the ground plane to improve impedance bandwidth. The challenge of mutual coupling be-

* Corresponding author: Ayyaz Ali (ayaz.phd@students.mcs.edu.pk).

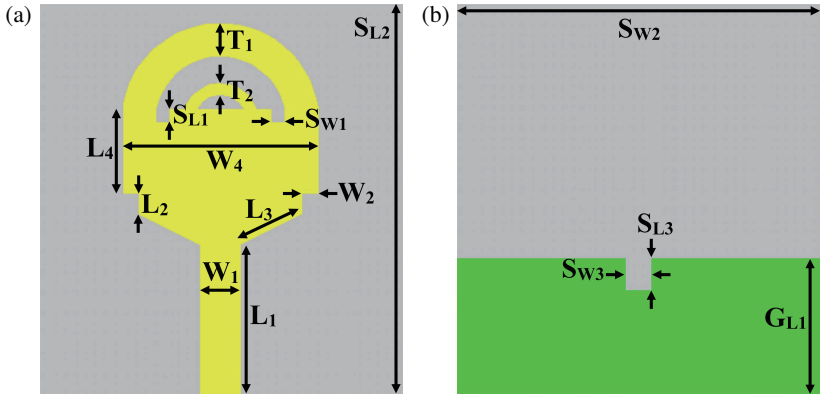

FIGURE 1. Geometrical dimensions of the single element antenna. (a) Front view, and (b) Back view.

tween individual elements in a MIMO antenna, particularly in the context of 5G frequency bands, has led to various mitigation techniques. Polarization diversity is employed in [7, 10, 12–15, 17]. [8] adopts a plus-shaped configuration for the four antenna elements to achieve high isolation, while [9] introduces a parasitic decoupling structure using thin striplines arranged in a plus shape. In contrast, [16] utilizes the un-protruded multi-slot technique within the ground structure for high isolation. Furthermore, study [18] applies a coating of ferrite material to the radiating element in an effort to reduce inter-element coupling, while study [19] incorporates twin L-shaped decoupling structures among the antenna elements, accompanied by three etched slots on the ground plane. The common ground structure serves as a shared reference voltage level for different signals, which is indispensable for any MIMO system. Its significance and advantages have been extensively discussed in the literature [13, 15, 16, 20]. Additionally, study [21] achieves high isolation by introducing a modified inter-digital capacitor (MIDC) between the radiating elements. The challenges of mutual coupling between the elements of MIMO antennas are thoroughly explored in the literature [22, 23], addressing various parameters used to measure mutual coupling and strategies for its minimization. Techniques, such as the slits etching approach, protruding ground stub structures, metamaterials, electromagnetic band gap (EBG) structures, cloaking structures, shorting vias and pins, are highlighted as effective means to reduce mutual coupling between MIMO antenna elements.

This paper presents a novel antenna design with the goal of enhancing impedance bandwidth and optimizing radiation patterns to improve performance in wireless communication applications. The proposed design features a rectangular microstrip patch radiator placed atop a gradually changing feedline structure. Additionally, two semicircles, each with distinct radius, are incorporated onto the patch radiator to provide a wider bandwidth. To further improve the impedance bandwidth, four slots are added on the radiator, and one slot is positioned at the top center of a partial ground plane on the backside of the substrate. This comprehensive approach enhances the antenna's suitability for diverse wireless communication applications. In order to demonstrate the practicality of the design, a 4×4 MIMO antenna configuration is formulated and tested, showcasing its efficacy in achieving enhanced isolation between antenna elements. This work represents a valuable contribution to the field, emphasizing the antenna's potential for widespread application in wireless communication scenarios.

2. FUNDAMENTAL ANTENNA DESIGN PROCEDURE

This section outlines the design and development of a single element antenna intended for the proposed MIMO antenna. The antenna was constructed using FR-4 material, with a substrate thickness of 1.6 mm and a copper thickness of 0.035 mm. The material characteristics include $\varepsilon_r = 4.3$ and $\tan(\delta) = 0.025$. The geometrical dimensions of the structure are illustrated in Fig. 1. Initially, a solitary rectangular patch was configured on the top side of the substrate, positioned on a 50 Ω transmission line. The feed line was gradually adjusted to connect with the radiating structure. Two square-shaped slits were etched near the feedline on the bottom edge of the radiator, and a partial ground plane was designed on the backside of the substrate. This design facilitated tri-band operation at 3.5–6.5 GHz, 9.5–13.5 GHz, and 17–19.5 GHz, as depicted in step 1 of Fig. 2. Subsequently, to enhance impedance bandwidth for the first and second bands, two semicircles were incorporated on top of the rectangle-shaped radiator. This modification resulted in an improved impedance bandwidth of 3–7.5 GHz and 9.5–14.5 GHz, as shown in step 2 of Fig. 2. Finally, to further augment the impedance bandwidth within the X-band and Ku-band, two square-shaped slits were etched on top of the rectangle-shaped radiator, and an additional slit was introduced on the top-middle section of the ground plane. This adjustment increased the bandwidth at the desired frequency bands, leading to operating frequencies of 3–7 GHz and 8–20 GHz, as presented in step 3 of Fig. 2. The proposed design of the single element antenna offers several advantages compared to a simple rectangular patch antenna. Notably, it provides flexibility in adjusting resonant frequencies for different frequency bands by modifying the inner or outer radius of the semicircles or adjusting the dimensions of the rectangular patch beneath these circles. Additionally, this design allows for wideband operation, surpassing the radiation characteristics of traditional simple rectangular microstrip patch antennas. The uti-

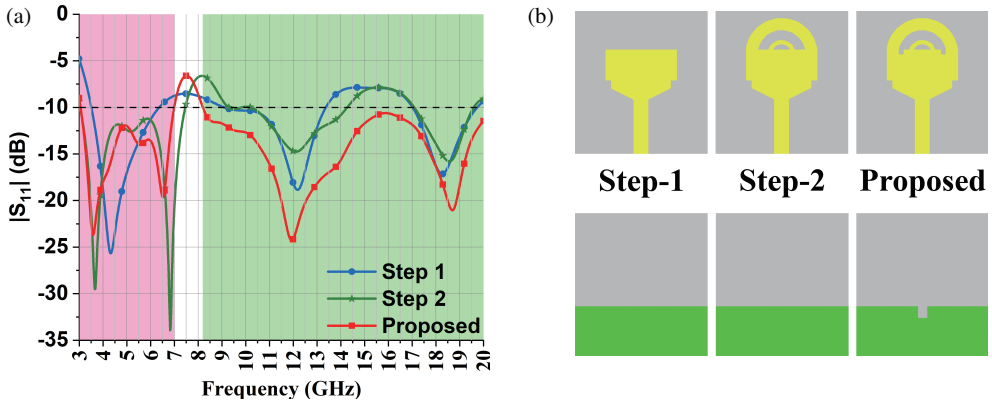

FIGURE 2. Development steps and comparison of reflection coefficient $|S_{11}|$ (dB) of the single element antenna.

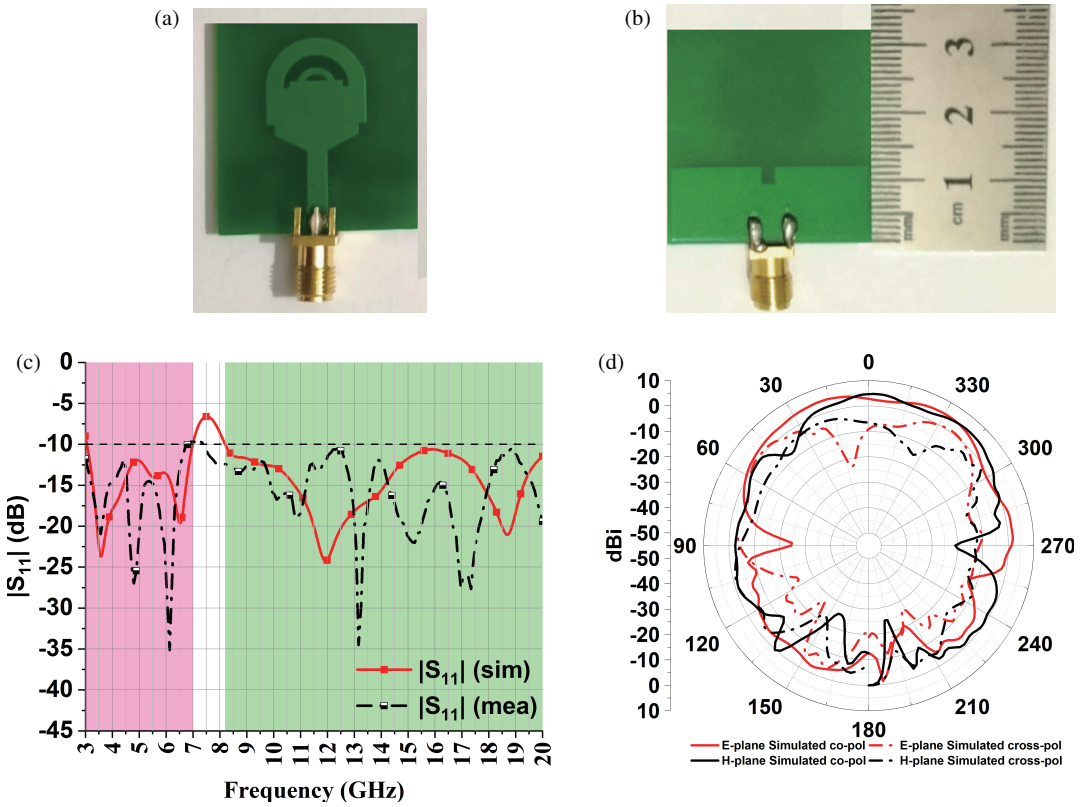

FIGURE 3. Test results of fabricated prototype of the proposed single element antenna, (a) front view, (b) back view, (c) comparison of simulated and measured reflection coefficients, and (d) Radiation pattern at 9.5 GHz.

lization of a partial ground structure is highly beneficial, enhancing impedance bandwidth, reducing interference between MIMO antenna elements, and simplifying the design and fabrication processes. These advantages significantly contribute to the overall performance and effectiveness of the antenna, ensuring superior signal transmission and reception within the desired frequency bands. Table 1 provides the dimensions of both the single and MIMO antennas.

The single element antenna was constructed using FR-4 material, and an SubMiniature version A (SMA)-type connector was soldered onto the antenna port, as depicted in Fig. 3. To evaluate the antenna's performance, a Vector Network Analyzer (Keysight ENA-E5080B) was employed for testing the fabricated antenna. The reflection coefficient $|S_{11}|$ (dB) within the operating frequency bands (3–7 GHz and 8–20 GHz) is observed to be below -10 dB. Its radiation pattern is also shown in Fig. 3(d). Minor discrepancies between the simulated and experimental results in Fig. 3 are attributed to tolerances in the fabrication and measurement setup [24].

3. DESIGN APPROACH FOR MIMO ANTENNA

The MIMO antenna expands from a single element antenna, employing duplication and orthogonal placement to create a

TABLE 1. Dimensions of proposed single element antenna and MIMO antenna.

Parameters	L_1	W_1	L_2	W_2	L_3	L_4
Values (mm)	11.5	3.0	1.63	1.25	5.31	6.5
Parameters	W_4	T_1	T_2	SL_1	SW_1	SL_2
Values (mm)	15.0	2.56	1.0	1.0	0.9	29.0
Parameters	SW_2	SL_3	SW_3	GL_1	SL_4	SW_4
Values (mm)	28.0	2.5	2.0	10.5	68.0	68.0
Parameters	D_1	DL_1	DW_1	IG_1	IG_2	R_1
Values (mm)	18.0	30.0	1.0	4.0	8.0	4.0

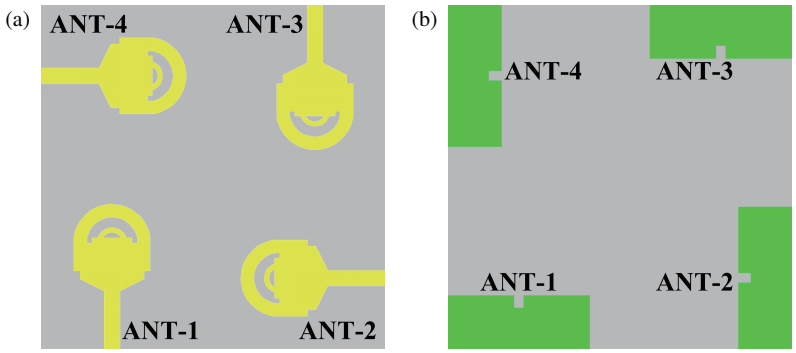

FIGURE 4. MIMO antenna configuration. (a) Front view, and (b) Back view.

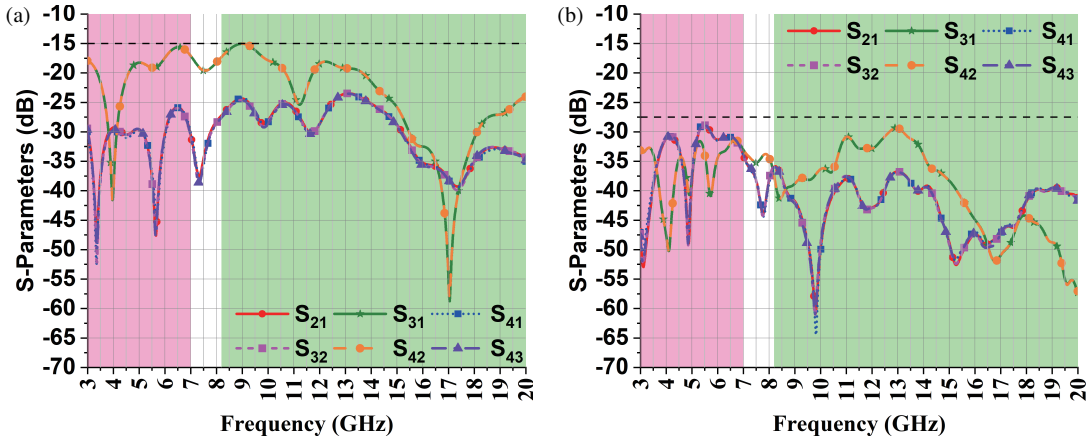

FIGURE 5. Effect of decoupling structure on isolation between MIMO antenna elements: (a) transmission coefficients without the decoupling structure and (b) transmission coefficients with the decoupling structure.

4×4 MIMO setup, as illustrated in Fig. 4. Simulation and testing of the MIMO antenna's transmission coefficients are depicted in Fig. 5(a), revealing low isolation between diagonal antenna elements (ANT 1–3 and ANT 2–4). This indicates potential high interference and suboptimal performance. To address this issue, a decoupling structure was necessary between antenna elements to enhance isolation in the MIMO configuration. The structure consists of two parallel long, thin microstrip lines connected by semicircle-shaped microstrip lines at the substrate's center. Two such structures are designed and positioned orthogonally to enhance isolation among all MIMO antenna elements, as illustrated in Fig. 6. This implementation improves isolation between inter-elements of the MIMO configuration, as demonstrated in Fig. 5(b), with enhanced levels below -27.5 dB. The proposed decoupling structure significantly boosts the isolation between antenna elements, resulting in an overall enhancement of MIMO antenna performance. This contributes to the reduction of signal noise and interference, ultimately elevating the antenna's effectiveness. It is worth noting that the addition of the decoupling structure did not increase the size of the proposed MIMO antenna. Detailed dimensions of the proposed MIMO antenna are provided in Fig. 6.

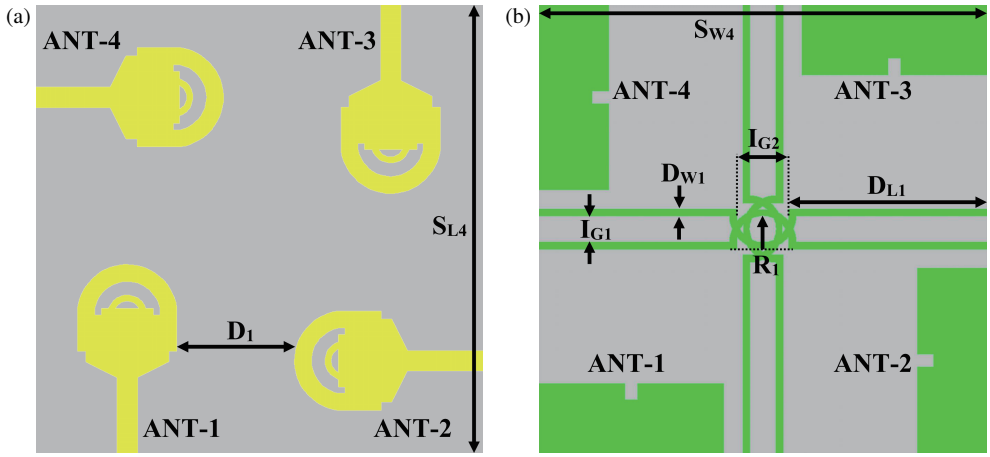

FIGURE 6. Dimensions of the proposed MIMO antenna with the decoupling structure: (a) Top view and (b) Bottom view.

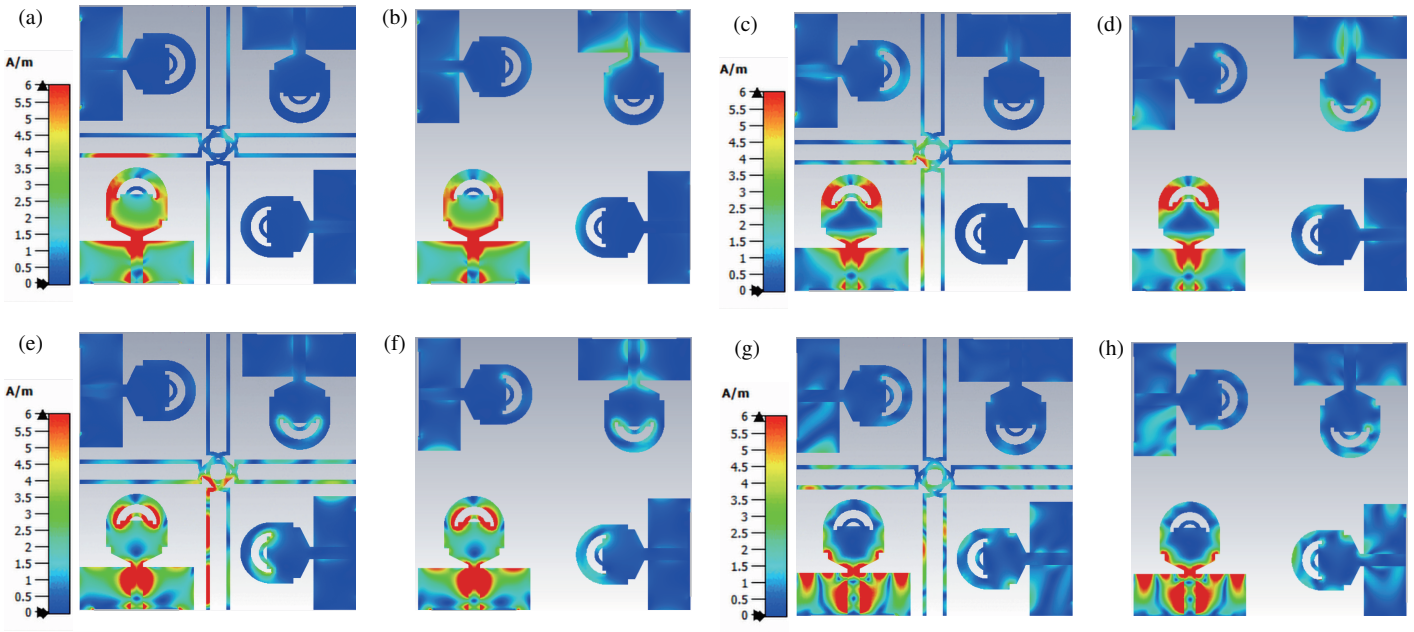

FIGURE 7. Simulated current distribution: (a) At 3.5 GHz with decoupler, (b) At 3.5 GHz without decoupler (c) At 6 GHz with decoupler, (d) At 6 GHz without decoupler (e) At 9.5 GHz with decoupler, (f) At 9.5 GHz without decoupler, (g) At 20 GHz with decoupler, and (h) At 20 GHz without decoupler.

3.1. Analysis of Surface Current Distribution of the Proposed MIMO Antenna

The proposed antenna's performance underwent evaluation through the simulation of surface current distribution on Port 1 at resonant frequencies, as illustrated in Fig. 7. This simulation facilitates the visualization of active components contributing to radiation and the effectiveness of the decoupling structure in reducing inter-element coupling. Achieving wideband operation involves designing a rectangle-shaped radiator joint connected to the feed line, featuring a gradually changing feed point. Upon exciting antenna 1, the maximum current density becomes observable around it, as depicted in Figs. 7(a)–(h). At 3.5 GHz, the maximum current concentration is observed around the edges of the rectangular-shaped patch and the semicircle atop antenna 1, with a wider radius, as shown in Fig. 7(a). Here, the role of the decoupling structure is evident in minimizing the coupling between the antenna elements. The coupling between diagonal antenna elements (ANT 1 and ANT 3) has been substantially reduced by the decoupling structure when comparing Fig. 7(a) and Fig. 7(b). This effective reduction in mutual coupling between the antenna elements can also be observed for other frequencies, as shown in Figs. 7(c)–(h). At 6 GHz, the most concentrated current density occurs within the semicircle, featuring a wider radius on antenna 1, as depicted in Fig. 7(c). Moving to 9.5 GHz, the most concentrated current density is observed on the semicircle, now with a smaller radius attached atop the rectangular-shaped patch of antenna 1, as shown in Fig. 7(e). Finally, at 20 GHz, the most concentrated current density occurs in proximity to the edges of the gradu-

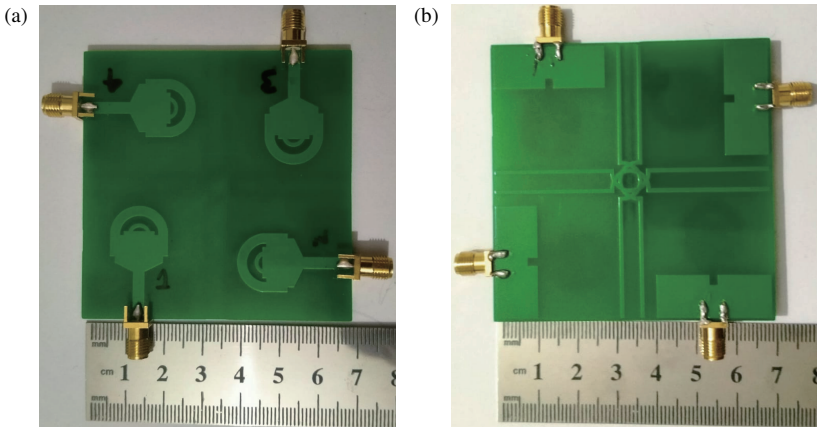

FIGURE 8. Fabricated MIMO antenna: (a) Top side, and (b) bottom side.

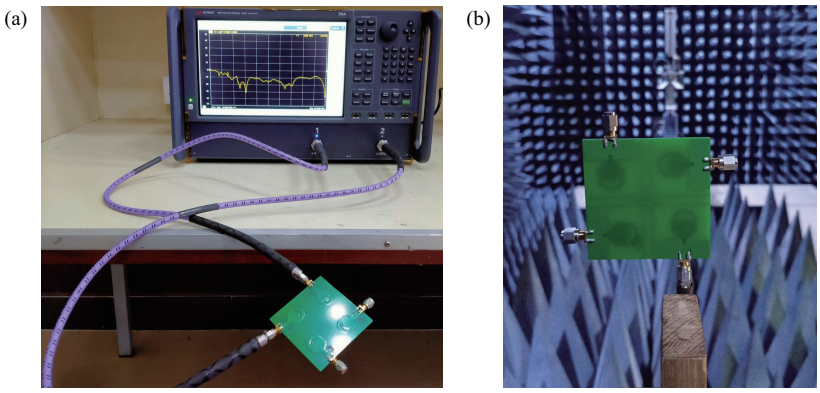

FIGURE 9. Test setup for measurement of transmission coefficients, reflection coefficients, and radiation patterns of the proposed MIMO antenna.

ally changing rectangular patch of antenna 1, as illustrated in Fig. 7(g).

4. RESULTS AND DISCUSSIONS

4.1. Fabricated Four-Element MIMO Antenna

The 4×4 MIMO antenna design was realized on an FR-4 substrate, and four SMA-type connectors were soldered onto the antenna ports, as illustrated in Fig. 8. Subsequently, the manufactured MIMO antenna underwent testing for reflection and transmission coefficients using a Vector Network Analyzer (Keysight ENA-E5080B), as shown in Fig. 9(a). During the measurement of the reflection coefficient ($|S_{11}|$), port 1 of the Vector Network Analyzer (VNA) was connected to antenna 1, while the remaining ports of the antennas were terminated using 50-ohm terminators. Similarly, the measurement of reflection coefficients ($|S_{22}|$, $|S_{33}|$, and $|S_{44}|$) was carried out in the same manner.

For the measurement of the transmission coefficient ($|S_{21}|$), port 1 of the VNA was connected to antenna 1, while port 2 of the VNA was connected to antenna 2. The remaining ports of the antenna were terminated using 50-ohm terminators. Similarly, the measurement of transmission coefficients ($|S_{31}|$, $|S_{41}|$, $|S_{23}|$, $|S_{24}|$, $|S_{34}|$) was carried out in the same manner.

4.2. Scattering Parameters

A Vector Network Analyzer (Keysight ENA-E5080B) is employed to measure the antenna's transmission and reflection coefficients. Initially, for the evaluation of antenna 1, its port was connected to the VNA, while the remaining antenna ports were terminated with 50 Ω terminators. The comparison and presentation of its simulated and experimentally measured data are illustrated in Fig. 10(a) and Fig. 10(b). Here, it can be observed that the simulated and laboratory-measured reflection coefficients $|S_{11}|$ (dB) exhibit good similarity. The reflection coefficients within the operating frequency bands (3–7 GHz, 8–15.4 GHz, and 18.7–20 GHz) are less than -10 dB, and the measured bandwidths are 4 GHz, 7.4 GHz, and 1.3 GHz for the first, second, and third bands, respectively.

To test the transmission coefficients $|S_{21}|$, $|S_{31}|$, $|S_{41}|$, $|S_{23}|$, $|S_{24}|$, and $|S_{34}|$, the VNA was connected to the two ports of the fabricated antenna, while the remaining two ports were terminated using 50 Ω terminators. Fig. 10(c) and Fig. 10(d) compare the simulated and experimental transmission coefficients, highlighting the significant improvement in inter-element isolation due to the proposed decoupling structure for the MIMO antenna. The comparison indicates that both the simulation results and laboratory-measured data show fair agreement for the transmission and reflection coefficients. Minor discrepancies between the simulated and experimental results in Figs. 10(a)–

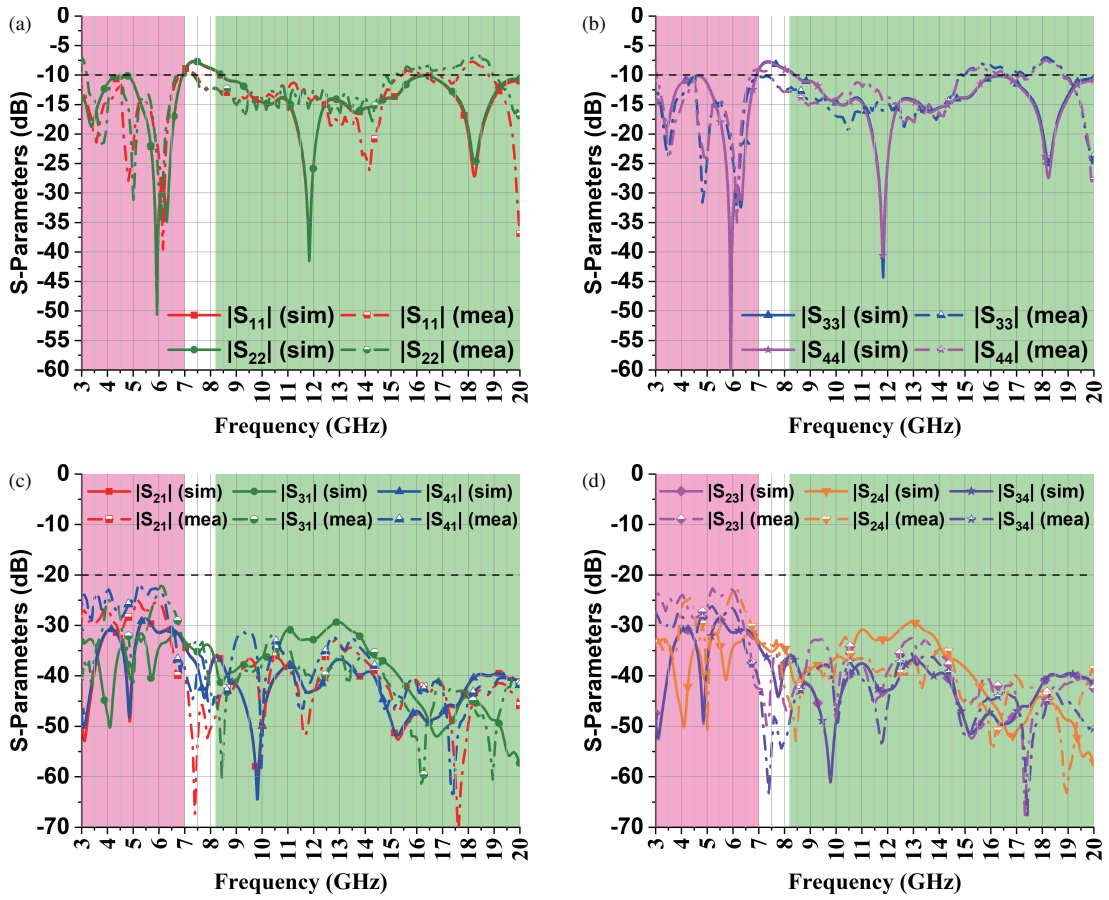

FIGURE 10. Contrast between simulated and experimental findings: (a) reflection coefficients ($|S_{11}|$ & $|S_{22}|$), (b) reflection coefficients ($|S_{33}|$ & $|S_{44}|$), transmission coefficients ($|S_{21}|$, $|S_{31}|$ & $|S_{41}|$), and (d) transmission coefficients ($|S_{23}|$, $|S_{24}|$ & $|S_{34}|$).

(d) are attributed to tolerances in the fabrication and measurement setup [24].

4.3. Radiation Patterns

Examining the radiation characteristics of the proposed MIMO antenna involves conducting measurements in a $9 \times 5 \times 5\,\text{m}^3$ NSI system based anechoic chamber, utilizing a driving software system with a turn-table mechanism. Fig. 9(b) illustrates the arrangement of the measurement setup in the anechoic chamber. The measurement process employs two antennas, with the MIMO antenna placed at the receiving end and connected to the measurement setup. A horn antenna, serving as the transmitting antenna, is strategically positioned in the line of sight to the proposed model and linked to a microwave source for excitation. Real-time measurement of radiation patterns is facilitated by the turn-table mechanism and associated software tool. Both E-plane and H-plane radiations are captured and presented in this section. Far-field E-plane and H-plane radiation patterns are measured, and a comparison between the simulated and measured patterns is depicted in Figs. 11(a)–(h). At 3.5 GHz, the maximum gain of 4.4 dBi is observed at $-34°$ as shown in Fig. 11(a), while at 6 GHz, the maximum gain of 4.25 dBi is observed at 338° as shown in Fig. 11(c), and at 9.5 GHz, the highest gain of 3.45 dBi occurs at 6° as shown in Fig. 11(e). Also, at 20 GHz, the maximum gain of 3.53 dBi is observed at 8° as shown in Fig. 11(g). Notably, the simulated and measured radiation patterns exhibit close agreement, with any discrepancies attributed primarily to cable losses and fabrication errors [24].

4.4. Gain and Radiation Efficiency

This section assesses the radiation performance of the fabricated 4×4 MIMO antenna. Gain measurements are conducted using the substitution method, wherein a calibrated laboratory antenna is connected to a source transmitting the signal. The developed antenna under test receives these signals, and the path loss is normalized to 0 dB to determine the actual gain. Experimental and simulated gains are illustrated in Fig. 12(a) and are observed to be in good agreement. In the frequency range of 3 GHz–7 GHz, the measured peak gain is 4.4 dBi at 3.5 GHz, while for the frequency range of 8 GHz–20 GHz, the measured peak gain is 6.23 dBi at 11.5 GHz.

To evaluate the antenna's efficiency, controlled power input is applied to Port 1 within an anechoic chamber [25]. The strength of the radiated electromagnetic field in the surrounding space is meticulously measured through a precisely calibrated setup facilitated by NSI2000 system software. The MIMO antenna's radiation efficiency is measured and compared to its

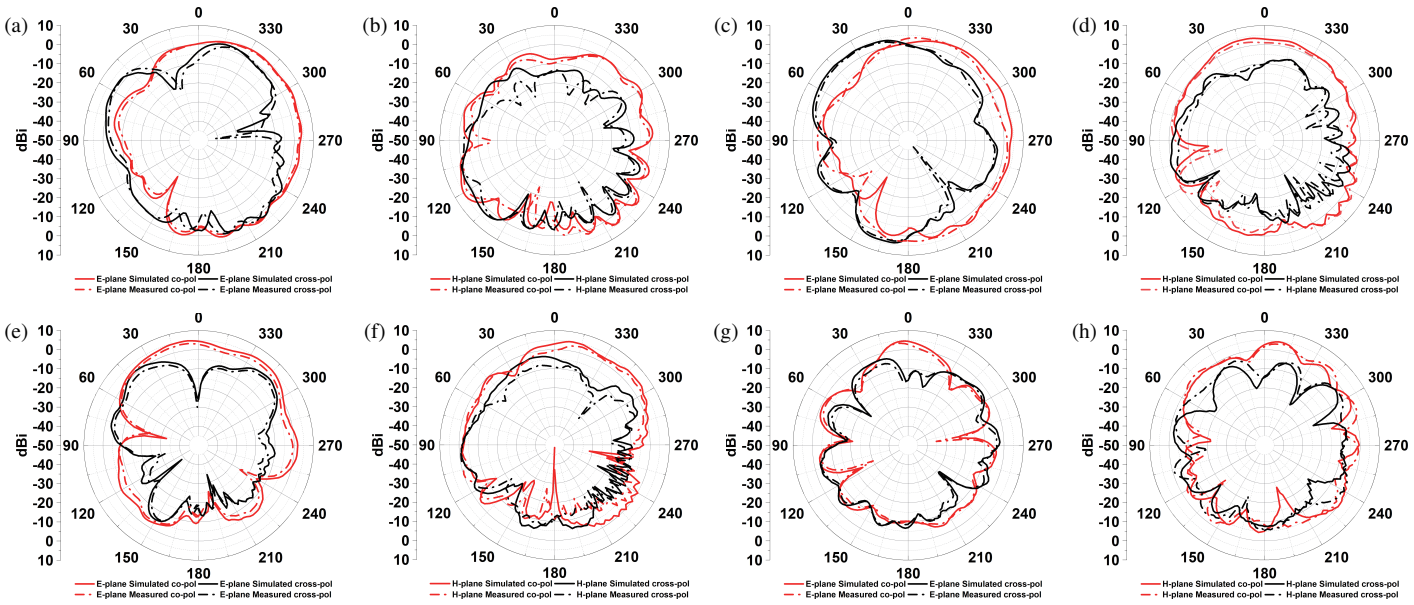

FIGURE 11. Comparison of simulation and experimental radiation patterns: (a) 3.5 GHz (E-plane), (b) 3.5 GHz (H-plane) (c) 6 GHz (E-plane), (d) 6 GHz (H-plane), (e) 9.5 GHz (E-plane), (f) 9.5 GHz (H-plane), (g) 20 GHz (E-plane), and (h) 20 GHz (H-plane).

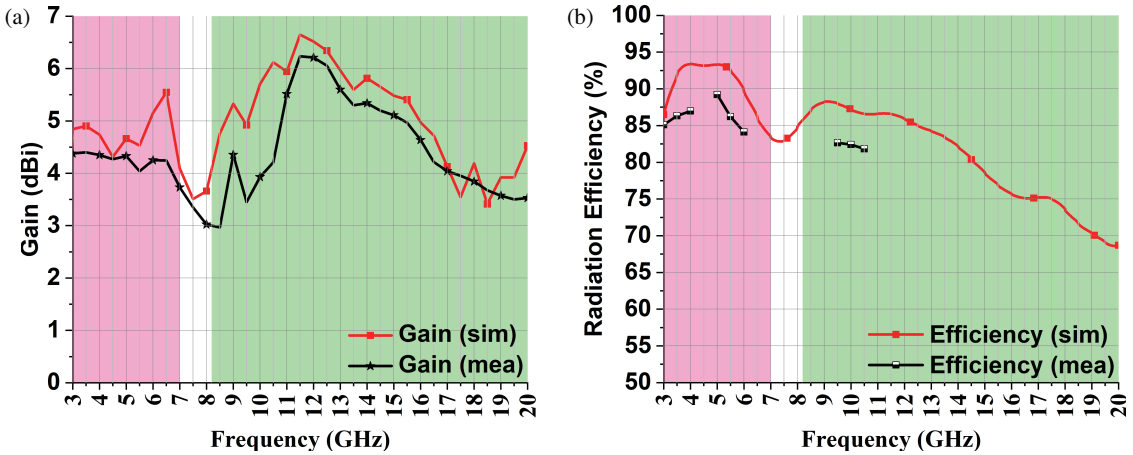

FIGURE 12. Contrast between simulated and experimental findings: (a) Gain and (b) Radiation Efficiency.

simulated values in Fig. 12(b), where it is found to be above 80% in the operating frequency bands.

5. PERFORMANCE EVALUATION OF THE FOUR-ELEMENT ANTENNA

To ascertain the effective performance of the four-element antenna, various parameters have been evaluated. The subsequent sections detail measurements of key parameters, encompassing the ECC, DG, TARC, and CCL.

5.1. Envelope Correlation Coefficient (ECC)

The ECC serves as a crucial metric in assessing the diversity performance within a MIMO setup, providing insights into the inter-element coupling in the MIMO system. Its computation relies on the radiation pattern [26], as articulated in Equation (1). In Equation (1), 'i' and 'j' denote the i^{th} and j^{th} antennas in the MIMO configuration, respectively, while 'φ' and 'θ' represent the azimuthal and elevation planes. Employing this equation, the ECC values for the proposed MIMO antenna were measured and are visually presented in Fig. 13(a). As illustrated in the figure, the measured ECC consistently registers values below 0.006, affirming the effective performance of the proposed antenna.

$$\mathrm{ECC}=\frac{\left|\iint E_{\theta i}\cdot E^{*}_{\theta j}+E_{\phi i}\cdot E^{*}_{\phi j}\right|^{2} d\Omega}{\iint (E_{\theta i}\cdot E^{*}_{\theta i}+E_{\phi i}\cdot E^{*}_{\phi i})d\Omega\cdot\iint (E_{\theta j}\cdot E^{*}_{\theta j}+E_{\phi j}\cdot E^{*}_{\phi j})d\Omega} \quad (1)$$

5.2. Diversity Gain (DG)

Within MIMO antennas, the implementation of a diversity scheme introduces a certain power loss during transmission.

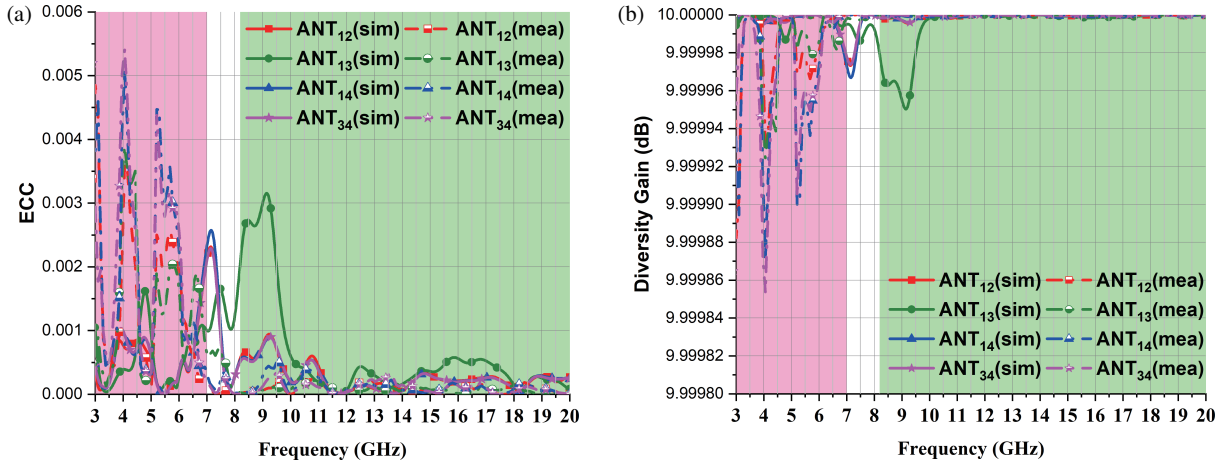

FIGURE 13. Contrast between simulated and experimental findings: (a) ECC and (b) DG.

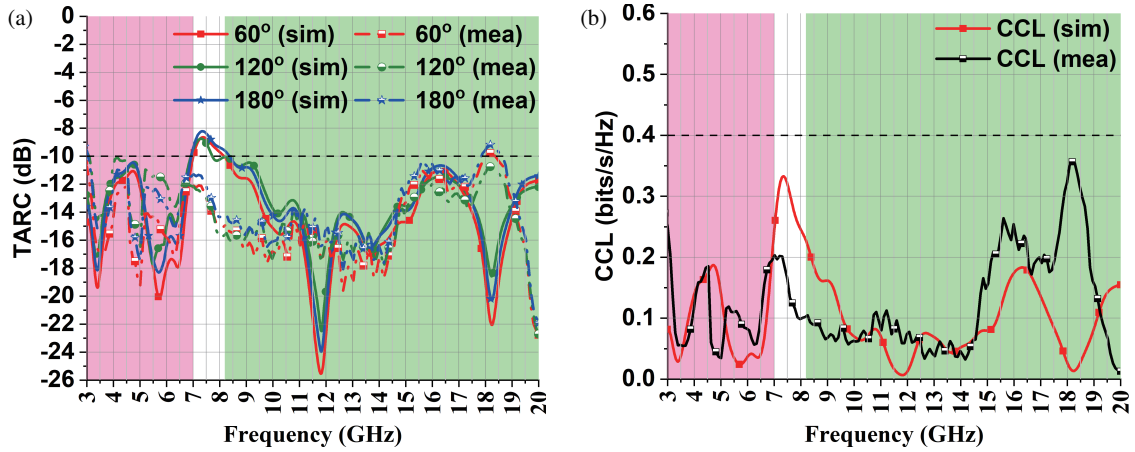

FIGURE 14. Contrast between simulated and experimental findings: (a) TARC, and (b) CCL.

This power loss is quantified by the diversity gain, as defined in Equation (2) from [27]. The simulated and computed diversity gain values, illustrated in Fig. 13(b), consistently exceed 9.99 dB. This underscores the exceptional performance of the antenna.

$$\mathrm{DG} = 10 \times \sqrt{1 - |\mathrm{ECC}|^2} \tag{2}$$

5.3. Total Active Reflection Coefficient (TARC)

The TARC stands as a widely recognized metric for assessing the radiation performance and bandwidth of a MIMO antenna. It is determined by comparing the incident input power with the reflected output power. The measurement of TARC is carried out using S-parameters, following equations (3) detailed in [28]. The depicted measured and simulated TARC values are presented in Fig. 14(a) for various phase angles (60°, 120°, and 180°). The outcomes reveal that the TARC remains below −10 dB across the entire operating bands.

$$\mathrm{TARC} = \frac{\sqrt{\sum_{i=1}^{N} |b_i|^2}}{\sqrt{\sum_{i=1}^{N} |a_i|^2}} \tag{3}$$

5.4. Channel Capacity Loss (CCL)

The CCL functions as a pivotal diversity parameter, influencing the upper limit of attainable communication transmission rates. To assess the CCL of the proposed MIMO antenna, Equation (4) from [25] was employed for measurement. The simulated channel capacity loss of the proposed MIMO antenna is compared with the actual measured outcomes in Fig. 14(b). The depicted data reveals that the measured channel capacity loss remains under 0.4 bits/s/Hz across the operational frequency bands, indicating compliance with acceptable limit conditions.

$$C_{\mathrm{loss}} = -\log_2 \det(\alpha^R) \tag{4}$$

where $\alpha^R = \begin{bmatrix} \alpha_{11} & \dots & \alpha_{14} \\ \vdots & \ddots & \vdots \\ \alpha_{41} & \dots & \alpha_{44} \end{bmatrix}$ and $\alpha_{ii} = 1 - \sum_{j=1}^{N} |S_{ij}|^2$.

Also, $\alpha_{ij} = -(S_{ij} \cdot S_{ij} + S_{ji} \cdot S_{ij})$

6. COMPARISON OF PROPOSED MIMO ANTENNA WITH THE LITERATURE

Table 2 presents a comparative analysis between the proposed MIMO antenna and existing literature on MIMO antennas.

TABLE 2. Comparative analysis between the proposed four-element antenna and the existing literature.

Ref.	No. of ANTs	MIMO ANT size (λ^2)	Operating Frequency (GHz)	Isolation without decouper (dB)	Isolation technique	Isolation after decoupler technique (dB)	Peak Gain (dBi)	Peak Efficiency (%)	ECC & DG	Inter-element spacing (λ)	Design complexity
[7]	4	0.6×0.6	3 – 11	<20	Orthogonal orientation	<20	3.4	70	<0.02 & >9.9	0.06	Simple
[8]	4	0.83×0.83	2.77 – 12	<15	Plus–shaped orientation	<15	5	80	<0.1 & >9.97	0.28	Simple
[9]	4	1.02×1.02	3.6 – 13.8	<12.7	Parasitic element	<15	4.8	NR	<0.01 & NR	0.30	Simple
[10]	4	0.39×0.39	2.9 – 13.6	<16	Polarization diversity	<16	5.8	93	<0.38 & >9.7	0.05	Simple
[11]	2	0.22×0.35	2.68 – 12.5	<15	Parasitic element	<20	5.2	90	<0.01 & NR	0.18	Simple
[12]	4	0.45×0.01	3.4 – 3.6 & 4.8 – 4.9	<8.5	Circular arrangement	<8.5	0.7	42.6	<0.26 & NR	0.02	Complex
[13]	4	0.86×0.86	3.22 – 3.97 & 4.95 – 5.51	<15	Orthogonal orientation	<15	5.5	95	<0.186 & >9.88	0.47	Simple
[14]	4	0.35×0.35	2.2 – 2.4, 3.3 – 3.6, & 4.7 – 6.2	<15	Orthogonal orientation	<15	2.9	88	<0.0086 & >9.99	0.12	Simple
[15]	4	0.36×0.36	4.36 – 6.90	<20	Orthogonal orientation	<20	2	90	<0.08 & >9.95	0.23	Simple
[16]	4	0.32×0.43	3.20 – 5.85	<10	un-protruded multi-slot	<20	3.5	85	<0.05 & >9.98	0.03	Simple
[17]	2	0.36×0.36	3.1 – 5.2	<10	Parasitic element	<15	2.6	90	<0.05 & >9.9	0.06	Simple
[18]	2	0.13×0.05	3.35 – 3.67	<6.6	Ferrite loading	<10.4	2	45.5	NR	0.02	Complex
[19]	2	0.28×0.28	3.4 – 3.6 & 5.15 – 5.85	<10	Slotted parasitic element	<16.7	2	80	<0.11 & >9.97	0.04	Simple
Prop	4	0.68×0.68	3.0 – 7.0, 8.0 – 15.4 & 18.7 – 20	<14	Defective slotted ground	<20	6.23	89	<0.006 & >9.99	0.18	Simple

*NR = Not Reported.

It is essential to highlight that the proposed antenna employs a greater number of antenna elements than [11, 17–19] and exhibits a more compact size than [8, 9, 13]. Furthermore, it demonstrates a larger bandwidth than [7–19] and greater isolation between antenna elements than [8–10, 12–14, 17–19]. The proposed MIMO antenna achieves higher gain values than [7–19], and higher radiation efficiency than [7, 8, 12, 14, 16, 18, 19]. Additionally, the proposed antenna displays lower values of ECC and comparable values of DG compared to [7–19]. Consequently, the proposed MIMO antenna can be considered suitable for the deployment in various wireless communication systems.

7. CONCLUSION

This paper introduces a wideband MIMO antenna designed to operate within the frequency ranges of 3 to 7 GHz, 8 to 15.4 GHz, and 18.7 to 20 GHz. The measured results closely align with the simulated outcomes. The antenna maintains reflection coefficients below −10 dB at the specified operating frequencies. The broad bandwidth is achieved through the implementation of gradual feedline adjustments, slots, and partial ground structure techniques. These methods not only widen the bandwidth but also enhance the antenna's radiation pattern across different frequencies. Notably, an impedance bandwidth of 4 GHz, 7.4 GHz, and 1.3 GHz is attained in the first, second, and third bands, respectively. To address interference concerns between the MIMO antenna elements, a novel decoupling structure is devised, resulting in high isolation of less than 20 dB across all operating frequency bands. This innovation minimizes interference, boosting overall efficiency. Peak gains of 4.4 dBi and 6.23 dBi at 3.5 GHz and 11.5 GHz, respectively, are attained. The radiation efficiency surpasses 80% across all operating frequency bands. The MIMO antenna's performance, assessed in terms of DG, ECC, TARC, and CCL, underscores its suitability for various wireless communication devices.

REFERENCES

[1] Luo, S., Y. Li, Y. Xia, and L. Zhang, "A low mutual coupling antenna array with gain enhancement using metamaterial loading and neutralization line structure," *The Applied Computational Electromagnetics Society Journal (ACES)*, 411–418, 2019.

[2] Li, M.-Y., Z.-Q. Xu, Y.-L. Ban, C.-Y.-D. Sim, and Z.-F. Yu, "Eight-port orthogonally dual-polarised MIMO antennas using loop structures for 5G smartphone," *IET Microwaves, Antennas & Propagation*, Vol. 11, No. 12, 1810–1816, 2017.

[3] Yuan, X.-T., W. He, K.-D. Hong, C.-Z. Han, Z. Chen, and T. Yuan, "Ultra-wideband MIMO antenna system with high element-isolation for 5G smartphone application," *IEEE Access*, Vol. 8, 56 281–56 289, 2020.

[4] Li, Q. L., S. W. Cheung, D. Wu, and T. I. Yuk, "Optically transparent dual-band MIMO antenna using micro-metal mesh conductive film for WLAN system," *IEEE Antennas and Wireless Propagation Letters*, Vol. 16, 920–923, 2016.

[5] Sui, J. and K.-L. Wu, "A self-decoupled antenna array using inductive and capacitive couplings cancellation," *IEEE Transactions on Antennas and Propagation*, Vol. 68, No. 7, 5289–5296, 2020.

[6] Alsariera, H., Z. Zakaria, and A. A. M. Isa, "A broadband p-shaped circularly polarized monopole antenna with a single parasitic strip," *IEEE Antennas and Wireless Propagation Letters*, Vol. 18, No. 10, 2194–2198, 2019.

[7] Ahmad, S., S. Khan, B. Manzoor, M. Soruri, M. Alibakhshikenari, M. Dalarsson, and F. Falcone, "A compact CPW-fed ultra-wideband multi-input-multi-output (MIMO) antenna for wireless communication networks," *IEEE Access*, Vol. 10, 25 278–25 289, 2022.

[8] Alharbi, A. G., U. Rafique, S. Ullah, S. Khan, S. M. Abbas, E. M. Ali, M. Alibakhshikenari, and M. Dalarsson, "Novel MIMO antenna system for ultra wideband applications," *Applied Sciences*, Vol. 12, No. 7, 3684, 2022.

[9] Andrade-González, E. A., J. A. Tirado-Méndez, H. Jardón-Aguilar, M. Reyes-Ayala, A. Rangel-Merino, and M. Pascoe-Chalke, "UWB four ports MIMO antenna based on inscribed Fibonacci circles," *Journal of Electromagnetic Waves and Applications*, Vol. 35, No. 9, 1202–1220, 2021.

[10] Khan, A. A., M. S. Khan, S. A. Naqvi, B. Ijaz, M. Asif, E. M. Ali, S. Khan, A. Lalbakhsh, M. Alibakhshikenari, and E. Limiti, "Printed closely spaced antennas loaded by linear stubs in a MIMO style for portable wireless electronic devices," *Electronics*, Vol. 10, No. 22, 2848, 2021.

[11] Tang, Z., J. Zhan, X. Wu, Z. Xi, L. Chen, and S. Hu, "Design of a compact UWB-MIMO antenna with high isolation and dual band-notched characteristics," *Journal of Electromagnetic Waves and Applications*, Vol. 34, No. 4, 500–513, 2020.

[12] Chang, L. and H. Wang, "Dual-band four-antenna module covering N78/N79 based on PIFA for 5G terminals," *IEEE Antennas and Wireless Propagation Letters*, Vol. 21, No. 1, 168–172, 2022.

[13] Dwivedi, A. K., A. Sharma, A. K. Singh, and V. Singh, "Design of dual band four port circularly polarized MIMO DRA for WLAN/WiMAX applications," *Journal of Electromagnetic Waves and Applications*, Vol. 34, No. 15, 1990–2009, 2020.

[14] Naidu, P. V., M. B. Dhanekula, K. M. Almustafa, A. Kumar, K. A. Meerja, and S. H. Akkapanthula, "Design and performance analysis of MAZE shaped quad port ACS fed tri band MIMO antenna for V2V and multi band applications," *AEU — International Journal of Electronics and Communications*, Vol. 134, 153676, 2021.

[15] Singh, A. K., A. K. Dwivedi, K. N. Nagesh, V. Singh, and R. S. Yadav, "Compact 4-port planar MIMO antenna with enhanced isolation for WLAN/WiMAX applications," *Sādhanā*, Vol. 47, No. 3, 138, 2022.

[16] Kulkarni, J., A. Desai, and C.-Y. D. Sim, "Wideband four-port MIMO antenna array with high isolation for future wireless systems," *AEU — International Journal of Electronics and Communications*, Vol. 128, 153507, 2021.

[17] Oliveira, J., G. D. Oliveira, A. G. D. Junior, V. P. S. Neto, and A. G. D'Assunção, "New compact MIMO antenna for 5G, WiMAX and WLAN technologies with dual polarisation and element diversity," *IET Microwaves, Antennas & Propagation*, Vol. 15, No. 4, 415–426, 2021.

[18] Wu, D., Y. Qiu, G. Yu, R. Guo, G. Wu, J. Wang, Y. Zhang, M. Zhu, and H.-M. Zhou, "Decoupling technique using ferrite-film loading for 5G MIMO applications," *International Journal of Antennas and Propagation*, Vol. 2022, Article ID 2028146, 2022.

[19] Paiva, S. B., A. G. D. Junior, V. P. S. Neto, and A. G. D'Assunção, "A new compact dual-polarized MIMO antenna using slot and parasitic element decoupling for 5G and WLAN applications," *Electronics*, Vol. 11, No. 13, 1943, 2022.

[20] Kumar, A., A. Q. Ansari, B. K. Kanaujia, J. Kishor, and S. Kumar, "An ultra-compact two-port UWB-MIMO antenna with dual band-notched characteristics," *AEU — International Journal of Electronics and Communications*, Vol. 114, 152997, 2020.

[21] Kumar, A., A. Q. Ansari, B. Kanaujia, J. Kishor, and N. Tewari, "Design of triple-band MIMO antenna with one band-notched characteristic," *Progress In Electromagnetics Research C*, Vol. 86, 41–53, 2018.

[22] Kumar, A., A. Q. Ansari, B. K. Kanaujia, J. Kishor, and L. Matekovits, "A review on different techniques of mutual coupling reduction between elements of any MIMO antenna. Part 1: DGSs and parasitic structures," *Radio Science*, Vol. 56, No. 3, 1–25, 2021.

[23] Kumar, A., A. Q. Ansari, B. K. Kanaujia, J. Kishor, and L. Matekovits, "A review on different techniques of mutual coupling reduction between elements of any mimo antenna. part 2: Metamaterials and many more," *Radio Science*, Vol. 56, No. 3, 1–22, 2021.

[24] Liu, L., Y. F. Weng, S. W. Cheung, T. I. Yuk, and L. J. Foged, "Modeling of cable for measurements of small monopole antennas," in *2011 Loughborough Antennas & Propagation Conference*, 1–4, 2011.

[25] Aghoutane, B., S. Das, M. E. Ghzaoui, B. T. P. Madhav, and H. E. Faylali, "A novel dual band high gain 4-port millimeter wave MIMO antenna array for 28/37 GHz 5G applications," *AEU — International Journal of Electronics and Communications*, Vol. 145, 154071, 2022.

[26] Vaughan, R. G. and J. B. Andersen, "Antenna diversity in mobile communications," *IEEE Transactions on Vehicular Technology*, Vol. 36, No. 4, 149–172, 1987.

[27] Desai, A., C. D. Bui, J. Patel, T. Upadhyaya, G. Byun, and T. K. Nguyen, "Compact wideband four element optically transparent MIMO antenna for mm-wave 5G applications," *IEEE Access*, Vol. 8, 194 206–194 217, 2020.

[28] Sharawi, M. S., "Printed multi-band MIMO antenna systems and their performance metrics [wireless corner]," *IEEE Antennas and Propagation Magazine*, Vol. 55, No. 5, 218–232, 2013.